Spontaneous supercurrent and φ_0 phase shift parallel to magnetized topological insulator interfaces

Mohammad Alidoust and Hossein Hamzehpour
Department of Physics, K. N. Toosi University of Technology, Tehran 15875-4416, Iran
(Received 9 June 2017; published 13 October 2017)

Employing a Keldysh-Eilenberger technique, we theoretically study the generation of a spontaneous supercurrent and the appearance of the φ_0 phase shift parallel to uniformly in-plane magnetized superconducting interfaces made of the surface states of a three-dimensional topological insulator. We consider two weakly coupled uniformly magnetized superconducting surfaces where a macroscopic phase difference between the s-wave superconductors can be controlled externally. We find that, depending on the magnetization strength and orientation on each side, a spontaneous supercurrent due to the φ_0 states flows parallel to the interface at the nanojunction location. Our calculations demonstrate that nonsinusoidal phase relations of current components with opposite directions result in maximal spontaneous supercurrent at phase differences close to π. We also study the Andreev subgap channels at the interface and show that the spin-momentum locking phenomenon in the surface states can be uncovered through density of states studies. We finally discuss realistic experimental implications of our findings.

DOI: 10.1103/PhysRevB.96.165422

I. INTRODUCTION

The topological insulator (TI) is a new state of matter with revolutionary prospects in topological superconducting spintronics and topological quantum computation [1,2]. The topological insulators rely mainly on strong spin-orbit couplings and possess conductive surfaces, while showing insulating aspects in their bulk. Subsequently, TIs provide unique realistic platforms to study robust quantum relativistic phenomena such as spin-momentum locking and quantum spin Hall effect [1,2].

The spin direction of a moving particle at the surface of a three-dimensional (3D) TI in the presence of time-reversal symmetry is rigidly locked to its momentum direction [1,2]. Due to the spin-momentum locking phenomenon, the induction of superconductivity and magnetism in the surface of a TI is predicted to serve as an unprecedented condensed matter platform that supports odd frequency, topological superconductivity, and Majorana fermions [3–12]. In order to fabricate superconducting and magnetic surface states, one can proximitize the surface channels with a superconductor and ferromagnet, respectively [14,15]. The proximity-induced superconductivity and magnetism in the surface states are externally controllable through manipulating their inductors. It is worth mentioning that the spin-orbit coupling in the presence of superconductivity and magnetism can result in intriguing spin-dependent phenomena in various materials even in systems with strong nonmagnetic scattering resources [16–23].

In recent experiments on the quantum transport through TI surface states reported by different groups, it has been concluded that a proper theoretical framework, describing all kinds of samples including disordered ones, is an approach that accommodates the possibility of the presence of nonmagnetic scatterings [5,7,24,25]. To provide such a theoretical framework, the quasiclassical approach in the equilibrium and nonequilibrium states was generalized for 3D TI surface states with different levels of the density of nonmagnetic impurities in the presence of superconductivity and magnetism with arbitrary magnetization patterns [26,27]. This approach was employed to study TI-based diffusive Josephson configurations involving chiral helical magnetizations and the Edelstine phenomenon at the surface states. It was theoretically shown that well-controlled 0-π supercurrent reversals, φ_0 junctions, and proximity-induced vortices [28] are accessible through the spin-momentum locking phenomenon and magnetoelectric effect [26,27]. Also, several works have demonstrated that the spin-momentum locking phenomenon in the surface states of 3D TI plays crucial roles independently of the amount of nonmagnetic impurities present in these channels [29–33].

The spontaneous surface flow of currents can occur in the context of ^{3}He-A superfluid [3,34]. Also, the unconventional superconductors in proper situations host surface states and spontaneous currents parallel to interfaces [34–46]. This phenomenon has theoretically been studied in several systems including Josephson junctions made of s-wave/d-wave superconductors with different crystallographic orientations, chiral superconductors, and ferromagnetic layers coupled to the unconventional superconductors [47–51]. Nonetheless, the experimental observation of spontaneous supercurrents at the surfaces of chiral superconductors is still elusive partially due to the Meissner effect and strong disorders that may exist at the surfaces [42–45].

In this paper, we make use of the Eilenberger equation derived in Ref. [26] to analyze supercurrent flows at the interfaces of uniformly magnetized superconducting surface states of 3D TIs. We consider a 2D Josephson weak-link configuration made of surface channels of a 3D TI with an externally controllable superconducting phase difference φ and uniform in-plane magnetizations in each segment depicted in Fig. 1. Note that the superconductivity inductor electrodes are spin-singlet superconductors. We show that when the magnetization strength within the left and right sides of the contact are unequal and perpendicular to the interface, a spontaneous supercurrent flows along the junction interface, where its direction and amplitude can be controlled through the extrinsic φ applied perpendicular to the interface. Our results demonstrate that the maximum value of the spontaneous current can be achieved at phase differences close to $\varphi = \pi$.

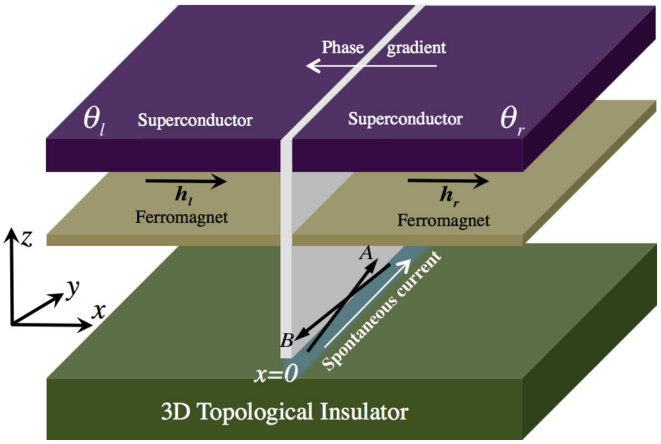

FIG. 1. Schematic of the TI-based Josephson weak-link junction considered. The superconductivity and magnetism are induced in the surface states of the 3D TI by virtue of the proximity effect. The macroscopic phases of the left and right superconductors $\theta_{l,r}$ can be controlled externally. The orientation of the uniform in-plane magnetization induced in the surface states $\boldsymbol{h}_{l,r}$ also can be calibrated through an external magnetic field. The left and right segments are separated by an insulator at $x = 0$, constituting an interface along the y axis. We assume that a phase gradient is applied across the junction normal to the interface and consider two trajectories in the xy plane, parallel with the interface, marked by A and B arrows to analyze the supercurrent flow parallel to the junction interface along the y axis.

We justify our findings by calculating the phase relation of spontaneous supercurrent components along two opposite trajectories parallel to the junction interface. The observation of the predicted spontaneous supercurrent is direct evidence of the rigid spin-momentum locking phenomenon in the surface states [25–27,29–31]. Furthermore, we calculate the density of states (DOS) at the interface and discuss how the strength and direction of magnetizations can alter Andreev bound states in such junctions that in turn reveal the role of strong spin-momentum locking in the surface states of a 3D TI.

The paper is organized as follows. We first explain the setup considered and derive proper Green's function describing the system in Sec. II. Next, using the Green's function obtained, we calculate the spontaneous supercurrent along the junction interface of the Josephson weak-link configuration and discuss the phase relation of its components. We also calculate the DOS and the Andreev subgap states for various values of φ and magnetization orientations. We support our numerical findings by Riccati-parametrizing the Green's function and deriving analytical expressions for the Andreev bound states in different situations. We finally give concluding remarks in Sec. III.

II. METHOD AND RESULTS

In order to analyze the spontaneous supercurrent flow along a uniformly in-plane magnetized interface made of surface channels of a 3D TI, we consider a Josephson weak-link shown in Fig. 1. The superconductivity and magnetism are both extrinsically induced in the surface states through s-wave spin-singlet superconductors and ferromagnetic thin films, respectively, and therefore can be calibrated externally. The Cooper pair wave function Ψ inside the ferromagnetic layer decays and oscillates as a function of location, i.e., $\Psi \propto \Delta \exp(-z/\xi_f)\cos(z/\xi_f)$, in which Δ is the superconducting order parameter inside the bulk superconductor and ξ_f is a characteristic length given by $\xi_f = \sqrt{D/h}$ in a diffusive ferromagnet with the diffusive constant D and exchange field h [15]. Thus, the thickness of the ferromagnetic layers should be properly chosen so that the superconductivity survives at the surface states. The orientation of magnetization induced in the surface channels $\boldsymbol{h}_{l,r}$ can be rotated by applying an external magnetic field [52]. To fabricate the double ferromagnetic setup depicted in Fig. 1, one can use different magnetic elements or compounds that respond differently to an externally applied magnetic field. For example, Py is a weak ferromagnet while LCMO is strong. When subjected to an external magnetic field, the magnetization of LCMO rotates reluctantly compared to Py [52] so this constitutes favorably misaligned magnetizations. The superconducting phase difference $\varphi = \theta_r - \theta_l$ can be controlled by passing a tuneable supercurrent through the top superconducting electrodes ($\theta_{l,r}$ are macroscopic phases of left and right superconductors). The two segments of the weak-link are separated by an insulator barrier along the y axis and the junction resides at $x = 0$.

To study the supercurrent flow in the weak-link Josephson structure, we follow Ref. [26], where the Usadel [53] and Eilenberger [54] techniques were generalized for the surface channels of a 3D TI in the presence of superconductivity and magnetism with different amounts of nonmagnetic impurities. Without losing the generality of our main conclusions, we utilize the Eilenberger equation [26] throughout the paper:

$$\frac{\alpha}{2}\{\hat{\boldsymbol{\eta}}, \nabla \check{g}\} = \left[\check{g}, \omega_n \hat{\tau}^z + i\boldsymbol{h}(\boldsymbol{r})\cdot\hat{\boldsymbol{\sigma}}\,\hat{\tau}^z + i\mu\hat{\boldsymbol{\eta}}\cdot\mathbf{n}_F + i\check{\Delta}(\boldsymbol{r}) + \frac{\langle\check{g}\rangle}{\tau}\right],$$
$$\check{g}(\omega_n, \boldsymbol{r}) = \begin{pmatrix} g(\omega_n,\boldsymbol{r}) & f(\omega_n,\boldsymbol{r}) \\ \tilde{f}(\omega_n,\boldsymbol{r}) & \tilde{g}(\omega_n,\boldsymbol{r}) \end{pmatrix}, \quad (1)$$

where $\hat{\boldsymbol{\eta}} = (-\hat{\sigma}^y, \hat{\sigma}^x)$, $\hat{\tau}^{\pm} = \hat{\tau}^x \pm i\hat{\tau}^y$, $\check{\Delta}(\boldsymbol{r}) = \hat{\sigma}^0(-\Delta(\boldsymbol{r})\hat{\tau}^+ + \Delta^*(\boldsymbol{r})\hat{\tau}^-)/2$, and $\boldsymbol{r}$ denotes the spatial dependence of quantities. The total Green's function $\check{g}$ has four components $f, g, \tilde{f}, \tilde{g}$ that determine the physical properties of a system. Here α represents the strength of the Rashba spin-orbit coupling available at the surface channels, $\boldsymbol{h}$ is the exchange field induced in the surface states, $\mathbf{n}_F = \mathbf{p}_F/|\mathbf{p}_F|$ is a unit vector in the direction of momentum $\mathbf{p}_F$ at the Fermi level, $\omega_n = (2n+1)\pi T$ is the Matsubara frequency, T is the temperature, and $n \in Z$. The vector $\hat{\boldsymbol{\sigma}}$ is composed of Pauli matrices and used for the spin space while $\hat{\boldsymbol{\tau}}$ denotes the particle-hole space. The parameter τ describes the mean-free-path time of moving quasiparticles in the presence of nonmagnetic impurities. Note that in the ballistic regime $1/\tau \to 0$ and to simplify our calculations we neglect the term $\langle g\rangle/\tau$ without losing the generality of our main conclusions. The Eilenberger equation (1) should be supplemented by a normalization condition, i.e., $\check{g}\check{g} = 1$, to provide correct solutions.

To appropriately describe the physics of the interface, we consider *Ansatz* of type $a_r^i + b_r^i e^{-k_r \boldsymbol{r}}$, $x > 0$ and $a_l^i + b_l^i e^{+k_l \boldsymbol{r}}$, $x < 0$ to the solutions of the Green's function components ($i = 1$–4 represents a specific component) on the

right and left sides of the weak-link, respectively [55–58]. We match the solutions at $x = 0$ where the two segments are weakly connected, derive analytically the corresponding Green's function, and eventually extract results by numerically integrating over the Matsubara frequency. To obtain $a^i_{l,r}$ and $b^i_{l,r}$ coefficients, we substitute the introduced *Ansatz* into the Eilenberger equation (1), make use of the normalization condition $\check{g}\check{g} = 1$, and assume that the solutions far enough away from the interface reduce to bulk solutions. Following this approach, we find suitable solutions to the components of the Green's function ($x > 0$):

$$g_r(\omega_n) = \frac{i\omega_n + h_r}{\sqrt{(i\omega_n + h_r)^2 - \Delta_r^2}} + b_r e^{-k_r \boldsymbol{r}}, \tag{2a}$$

$$f_r(\omega_n) = \frac{\Delta_r}{\sqrt{(i\omega_n + h_r)^2 - \Delta_r^2}} + \frac{2b_r \Delta_r e^{-k_r \boldsymbol{r}}}{2(i\omega_n + h_r) - i\alpha_r k_r}, \tag{2b}$$

$$\tilde{f}_r(\omega_n) = \frac{-\Delta_r^*}{\sqrt{(i\omega_n + h_r)^2 - \Delta_r^2}} - \frac{2b_r \Delta_r^* e^{-k_r \boldsymbol{r}}}{2(i\omega_n + h_r) + i\alpha_r k_r}, \tag{2c}$$

$$\tilde{g}_r(\omega_n) = \frac{-i\omega_n - h_r}{\sqrt{(i\omega_n + h_r)^2 - \Delta_r^2}} - b_r e^{-k_r \boldsymbol{r}}, \tag{2d}$$

in which wave vector $k_r = 2\alpha_r^{-1}\sqrt{-(i\omega_n + h_r)^2 + \Delta_r^2}$. To find solutions in the left segment $x < 0$, it suffices we follow the same procedure with replacing $k \to -k$ and indices $r \to l$. A generic solution at the interface can be given by invoking indices l,r for the Green's function and parameters involved on the left and right sides of the junction shown in Fig. 1.

By matching the Green's function of the left and right segments of the weak-link at the junction location $x = 0$, the Green's function of the interface $\check{g}$ can be expressed by the following g and f components:

$$g(\omega_n) = \frac{\alpha_r k_r \Omega_l \Delta_r e^{i\theta_r} i\omega_n (i\omega_n + h_l)[\alpha_l k_l - 2i(i\omega_n + h_l)] + \alpha_l k_l \Omega_r \Delta_l e^{i\theta_l} i\omega_n (i\omega_n + h_r)[2(i\omega_n + h_r) - i\alpha_r k_r]}{2\Omega_l \Omega_r (i\omega_n + h_l)(i\omega_n + h_r)\{\Delta_l e^{i\theta_l}[2(i\omega_n + h_r) - i\alpha_r k_r] - \Delta_r e^{i\theta_r}[2(i\omega_n + h_l) + i\alpha_l k_l]\}}, \tag{3a}$$

$$f(\omega_n) = \frac{-\omega_n \Delta_r \Delta_l e^{i(\theta_r + \theta_l)}\{\alpha_r k_r (i\omega_n + h_l)\Omega_l + \alpha_l k_l (i\omega_n + h_r)\Omega_r\}}{\Omega_l \Omega_r (i\omega_n + h_l)(i\omega_n + h_r)\{\Delta_r e^{i\theta_r}[+i\alpha_l k_l + 2(i\omega_n + h_l)] - \Delta_l e^{i\theta_l}[-i\alpha_r k_r + 2(i\omega_n + h_r)]\}}, \tag{3b}$$

$$\Omega_{l,r} = \sqrt{\Delta_{l,r}^2 + \omega_n^2}, \quad k_{l,r} = \frac{2}{\alpha_{l,r}}\sqrt{\Delta_{l,r}^2 - (i\omega_n + h_{l,r})^2}.$$

Because of the charge conservation law, the Green's function at the interface, i.e., $x = 0$, is sufficient to study the supercurrent and thus we restrict our attention to $\check{g}(x = 0)$. Note that the spatial dependence of the total Green's function is given by Eqs. (2a)–(2d). The charge supercurrent is given through the g component of the total Green's function:

$$\boldsymbol{J}_e(\boldsymbol{r}) = 2ie\pi T N(0) \sum_{n \in Z} \langle \boldsymbol{v}_F g(\omega_n, \boldsymbol{r}) \rangle, \tag{4}$$

where the average $\langle \ldots \rangle$ is taken over the direction of momentum, $\boldsymbol{v}_F$ is the Fermi velocity, and $N(0)$ the density of states at the Fermi level.

To gain insight, let us first assume that $h_{l,r} = 0, \theta_l = -\varphi/2$, $\theta_r = +\varphi/2$, and $\Delta_r \neq \Delta_l$. In this case, we find the following current phase relation to the supercurrent flowing in the x direction:

$$J_e^x = 2e\pi T N(0) \times \sum_{n \in Z} \frac{\Delta_r \Delta_l \sin\varphi}{\omega_n^2 + \sqrt{(\omega_n^2 + \Delta_r^2)(\omega_n^2 + \Delta_l^2)} + \Delta_r \Delta_l \cos\varphi}. \tag{5}$$

As seen, the supercurrent in the x direction is *directly* proportional to the order parameter of the left and right superconductors, i.e., Δ_l and Δ_r. Therefore, if one of the gaps is directional dependent, for example in a $d_{x^2-y^2}$-wave superconductor [i.e., Δ_l (or Δ_r) $= \Delta_0 \cos 2(\theta - \chi)$ where $v_x = |\boldsymbol{v}_F| \cos\theta$ is the particle velocity in the x direction and χ is the angle that the d-vector makes with respect to an axis normal to the interface], we see that the supercurrent along the A and B trajectories (shown in Fig. 1) can be unequal in amplitude when $\varphi \neq 0$. This implies that a finite spontaneous supercurrent can flow along the interface when a nonzero superconducting phase difference is applied perpendicular to the junction interface in the x direction, i.e., $\varphi \neq 0$ [47].

Let us return to the main structure we are interested in, namely, a magnetized junction where superconductivity is s-wave spin-singlet and not directional dependent. We first consider a simple case where $\Delta_r = \Delta_l = \Delta$ and $h_l = 0$. Figure 2 exhibits the total spontaneous supercurrent $J^{\rm tot}$ at the junction $x = 0$ along the y axis parallel to the interface as a function of the superconducting phase difference between the left and right segments $\varphi = \theta_r - \theta_l$. In our calculations, we have assumed that the phase difference is controllable and uniform along the y axis, and neglected the influences of boundaries along the y axis. The former assumption can be understood by noting that the superconductivity is induced in the surface states by an external electrode so that one can control its macroscopic phase via the injection of a supercurrent. The latter assumption is valid in a system where the junction is wide enough compared to the superconducting coherence length so that the boundaries in the y direction are located in infinity [21,22,26–28,59]. As seen in Fig. 2, $J^{\rm tot}$ vanishes when the magnetization strength is zero $h_r = 0$. By increasing the magnetization strength, $J^{\rm tot}$ is enhanced, and eventually, further increase in h_r suppresses $J^{\rm tot}$. The amplitude of the spontaneous current reaches its maximum for all values of h_r in phase differences close to $\varphi = \pi$. Also, the spontaneous current along the interface changes sign before and after $\varphi = \pi$. To understand the behaviors of the spontaneous supercurrent $J^{\rm tot}$ parallel to the interface at $x = 0$, we calculate the components of total current. To this end, the

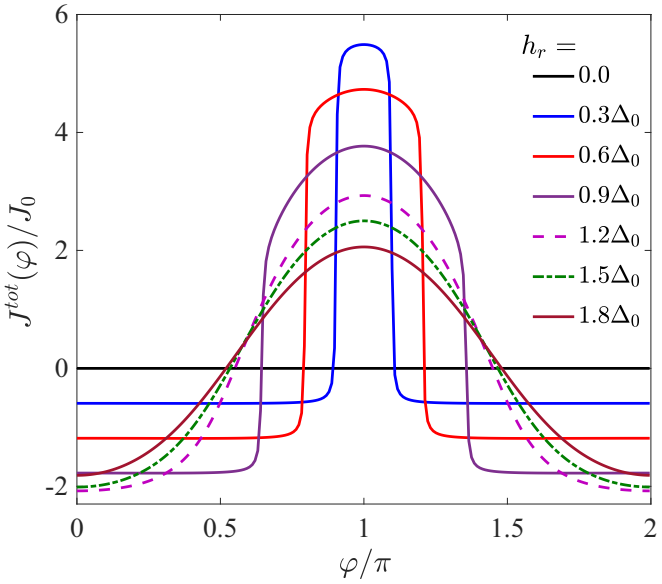

FIG. 2. Total supercurrent (spontaneous current) at the junction location $x = 0$, displayed in Fig. 1, along the y axis as a function of phase gradient perpendicular to the junction $\varphi = \theta_r - \theta_l$. The magnetization in the left segment is assumed zero $h_l = 0$ while the magnetization in the right segment is directed along the x axis normal to the interface and its strength varies from $h_r = 0$ to $1.8\Delta_0$.

current densities along opposite trajectories A and B parallel to the interface, shown in Fig. 1, should be calculated so that the total spontaneous current is given by $J^{\rm tot} = J^A - J^B$. To simplify the current density phase relations and derive an analytical expression, we set $\Delta_l = \Delta_r = \Delta$, $h_l = 0$, and $h_r \neq 0$ (however, in our numerical calculations, all quantities are assumed nonzero that result in long expressions and therefore we avoid presenting them). The supercurrent density along the A trajectory is expressed by

$$J = J_0 \sum_{n\in Z} \frac{2\mathcal{Z}\{\mathcal{S}_1 \sin(\varphi_0^r + \varphi) - \omega_n \sin\varphi + h_r \cos\varphi\}}{\mathcal{D}}, \quad (6)$$

$$\begin{aligned}\mathcal{D} = &-2\{h_r(\mathcal{Z}\sin\varphi - \mathcal{S}_1 \sin\varphi_0^r) + \mathcal{S}_1\omega_n \cos\varphi_0^r\} \\ &+ 2\mathcal{S}_2\mathcal{Z}\cos(\varphi_0^r + \varphi) - 2\omega_n\mathcal{Z}\cos\varphi \\ &+ 2\omega_n\sqrt{\Delta^2 + \omega_n^2} + \Delta^2 + h_r^2 \\ &+ \sqrt{(\Delta^2 + \omega_n^2)^2 + h_r^4 + 2h_r^2(\omega_n^2 - \Delta^2)} + 3\omega_n^2, \quad (7a)\end{aligned}$$

$$w\mathcal{S}_1 = \left[2\omega_n^2(\Delta^2 + h_r^2) + (h_r^2 - \Delta^2)^2 + \omega_n^4\right]^{\frac{1}{4}}, \quad (7b)$$

$$\mathcal{S}_2 = \left[(\Delta^2 + \omega_n^2)^2 + h_r^4 + 2h_r^2(\omega_n^2 - \Delta^2)\right]^{\frac{1}{4}}, \quad (7c)$$

$$\varphi_0^r = \frac{1}{2}\arg[\Delta^2 - (h_r + i\omega_n)^2], \quad (7d)$$

$$\mathcal{Z} = \sqrt{\Delta^2 + \omega_n^2} + \omega_n. \quad (7e)$$

A phase relation similar to Eq. (6) can be obtained for the current density along the B trajectory by properly accounting for the magnetization direction. Figure 3(a) illustrates the spontaneous current densities along trajectories A and B as a

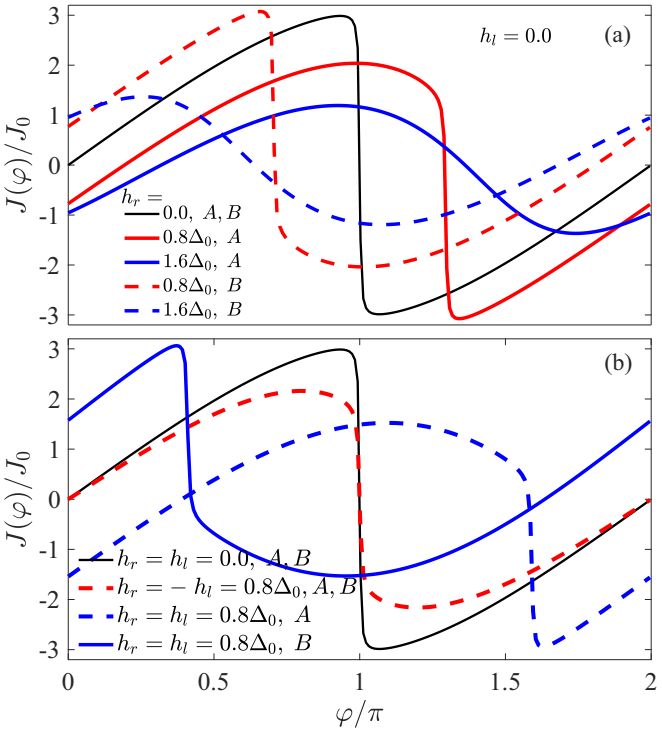

FIG. 3. Supercurrent densities along A and B trajectories parallel to the interface shown in Fig. 1 as a function of phase difference perpendicular to the junction interface φ. In panel (a) we set $h_l = 0$ and vary h_r while in panel (b) we consider situations where $h_r = \pm h_l$.

function of φ for three different values of $h_r = 0, 0.8\Delta_0, 1.6\Delta_0$, and $h_l = 0$. Here we have defined $J_0 = 2e\pi T N(0)$. Note that the magnetization is oriented along the x axis perpendicular to the junction interface. As seen, the current densities along the A and B trajectories are identical when $h_r = 0$. This is starkly oppose to the cases where $h_r \neq 0$. We see that the current densities along the A and B trajectories are dissimilar and therefore cause a finite spontaneous current along the interface $J^{\rm tot} = J^A - J^B \neq 0$. From Fig. 3(a) it is clear that $J^{\rm tot}$ is at a maximum at phases close to $\varphi = \pi$ due to the nonsinusoidal behavior of the current density phase relations. The current densities are nonzero at zero phase difference when $h_r \neq 0$; namely the current density experiences a φ_0 phase shift in the presence of magnetization. From Eq. (6) it is apparent that the current density is nonzero at zero phase difference $\varphi = 0$ when $h_r \neq 0$. It is worth mentioning that the appearance of a φ_0 phase shift in the supercurrent has theoretically been discussed in various situations [13,16,26,27,60–70] and observed in experiments [71,72]. In structures where the spin-orbit meditated coupling is available, its interplay with a properly oriented Zeeman(-like) field results in a supercurrent flow perpendicular to the junction interfaces at zero phase difference [13,16,26,27,69,70]. Figure 3(b) illustrates the current densities along the A and B trajectories where the magnetizations in both sides of the weak-link are nonzero. We see that when $h_r = -h_l$, i.e., the magnetizations are equal in strength and oppositely oriented perpendicular to the interface, the current densities along the A and B trajectories are identical and hence the total spontaneous current along the

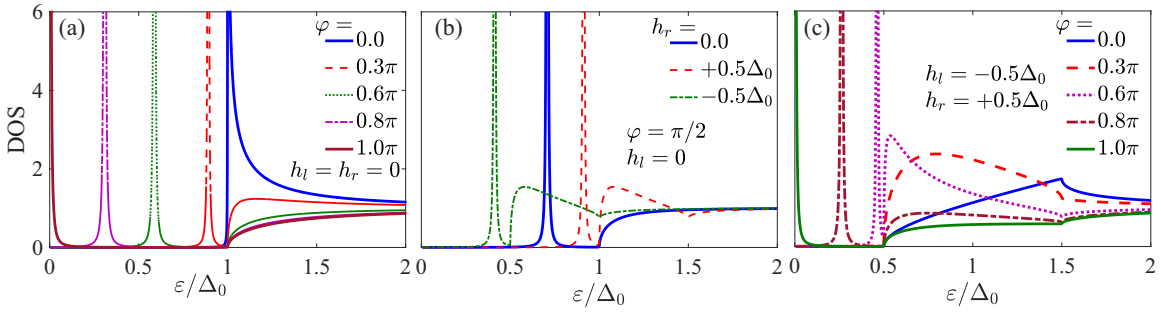

FIG. 4. The density of states DOS(ε) as a function of the quasiparticles energy ε at the interface of weak-link $x = 0$. (a) We set $h_r = h_l = 0$ and vary the phase difference $\varphi = 0, 0.3\pi, 0.6\pi, 0.8\pi, \pi$. In panel (b), we examine the effect of magnetization direction on the Andreev subgap states by setting $h_l = 0$, $\varphi = \pi/2$, and $h_r = 0, \pm 0.5\Delta_0$. (c) We consider opposite magnetization directions with identical intensities on the left and right sides of the weak-link $h_l = h_r = 0.5\Delta_0$ and vary the phase difference similarly to panel (a).

interface in the y direction vanishes similarly to the nonmagnetized case $h_r = h_l = 0$. The spontaneous current however reappears when $h_r = h_l$, namely, when the magnetizations of both sides are oriented in the same direction and perpendicular to the interface. From Fig. 3(b) it is clear that the current densities as a function of φ along the A and B trajectories are different if $h_r \neq 0$, and therefore it causes a finite spontaneous current parallel to the interface. Comparing Figs. 3(a) and 3(b), we conclude that a finite J^{tot} is also feasible even in a case where h_r and h_l have opposite orientations. The finite J^{tot} in this case is accessible when the magnetizations have different strengths, i.e., $|\boldsymbol{h}_r| \neq |\boldsymbol{h}_l|$. Our numerical calculations (not shown) also confirm this fact.

One of the measurable physical quantities in the laboratory is the density of states. The DOS can be detected by STM experiments or through I-V characteristic curves in a tunneling spectroscopy experiment where dI/dV is proportional to the DOS. The DOS in the quasiclassical approach is accessible through the normal component of the total Green's function, i.e., Eq. (3a):

$$\text{DOS}(\varepsilon, \boldsymbol{r}) = N(0) \operatorname*{Re}_{\delta \to 0} \{g(i\omega_n \to \varepsilon + i\delta, \boldsymbol{r})\}, \tag{8}$$

in which we have introduced an infinitesimal imaginary number $i\delta$ and, for convenience in our subsequent analyses, turn to the energy representation by substituting $i\omega_n \to \varepsilon + i\delta$. The imaginary part $i\delta$ helps to account properly for the Green's function poles. In Fig. 4 we plot the DOS as a function of normalized quasiparticle energy ε/Δ_0 at the interface $x = 0$. Figure 4(a) illustrates the DOS where the phase difference φ between the two segments of the Josephson weak-link (see Fig. 1) is $0, 0.3\pi, 0.6\pi, 0.8\pi, \pi$. We also set $h_l = h_r = 0$ which is equivalent to a normal Josephson contact. At $\varphi = 0$, the DOS shows the usual BCS gap structure with a singularity at $\varepsilon = \Delta_0$. When we set $\varphi \neq 0$ a singularity appears at energies below the superconducting gap $\varepsilon < \Delta_0$. This singular point corresponds to an Andreev bound state due to the resonance of particle-hole conversions at the interfaces of left and right superconductors. The bound state moves to $\varepsilon = 0$ when the phase difference is maximum $\varphi = \pi$. In Fig. 4(b), we set $h_l = 0$, $\varphi = \pi/2$ and plot DOS for $h_r = 0, \pm 0.5\Delta_0$. As seen, the nonzero magnetization in the right segment of weak-link shifts the Andreev subgap state to smaller or larger energies, depending on the magnetization direction. If we set opposite magnetization directions with identical strengths on opposite sides of the weak-link segments, i.e., $h_l = -h_r$, the shift in the Andreev bound states induced by the direction of magnetization disappears and the Andreev subgap state at $\varphi = \pi$ reoccurs at $\varepsilon = 0$.

To gain better insights, in what follows, we parametrize the Green's function and derive an analytical expression for the Andreev bound states. To this end, we make use of a so-called Riccati parametrization scheme [73] and define two propagators γ and $\tilde{\gamma}$ so that the Green's function is rewritten as follows:

$$\check{g} = \frac{1}{1 - \gamma\tilde{\gamma}} \begin{pmatrix} 1 + \gamma\tilde{\gamma} & +2\gamma \\ -2\tilde{\gamma} & -1 - \tilde{\gamma}\gamma \end{pmatrix}. \tag{9}$$

Substituting the parametrized Green's function into the Eilenberger equation, Eq. (1), two decoupled first-order differential equations for γ and $\tilde{\gamma}$ appear. After some calculations, we find the following solutions to γ and $\tilde{\gamma}$ at the interface from the right side of the weak-link $x \to 0^+$:

$$\gamma_r = \frac{(\varepsilon + h_r) - \text{sgn}(\varepsilon + h_r)\sqrt{(\varepsilon + h_r)^2 - \Delta_r^2}}{\Delta_r e^{-i\theta_r}}, \tag{10a}$$

$$\tilde{\gamma}_r = \frac{(\varepsilon + h_r) - \text{sgn}(\varepsilon + h_r)\sqrt{(\varepsilon + h_r)^2 - \Delta_r^2}}{\Delta_r e^{+i\theta_r}}. \tag{10b}$$

Similar solutions are derived to γ and $\tilde{\gamma}$ at the interface from $x \to 0^-$. The Andreev bound states can be determined through the singularities in the normal component of the Green's function as discussed earlier [see Eq. (8) and its associated results presented in Fig. 4]. Therefore, the singularities are solutions of $1 - \gamma\tilde{\gamma} = 0$ that result in

$$\cos\varphi - \frac{(h_l + \varepsilon)(h_r + \varepsilon)}{\Delta_l \Delta_r} + \left[\left\{1 - \left(\frac{h_l + \varepsilon}{\Delta_l}\right)^2\right\} \times \left\{1 - \left(\frac{h_r + \varepsilon}{\Delta_r}\right)^2\right\}\right]^{-\frac{1}{2}} = 0, \tag{11}$$

where we invoked the left and right indices l,r for the quantities of the left and right segments of the weak-link. By carrying out some calculations, we find the following relation

to the Andreev bound states:

$$\varepsilon_{\mathcal{A}} = \frac{h_r\Delta_l^2 + h_l\Delta_r^2 - \mathcal{H}_+\Delta_l\Delta_r\cos\varphi \pm \Delta_l\Delta_r\sin\varphi\sqrt{\Delta_l^2+\Delta_r^2-2\Delta_l\Delta_r\cos\varphi-\mathcal{H}_-^2}}{\Delta_l^2+\Delta_r^2-2\Delta_l\Delta_r\cos\varphi}, \tag{12}$$

in which we have defined $\mathcal{H}_\pm = h_l \pm h_r$ and $\varepsilon_{\mathcal{A}}$ determines the energy of the Andreev bound states. The supercurrent flow passes through these subgap bound states. Hence, the associated supercurrent phase relationship is proportional to the derivative of the bound state energies with respect to the phase difference, namely, $J \propto \sum_{\mathcal{A}} \frac{d\varepsilon_{\mathcal{A}}}{d\varphi}\tanh\beta\varepsilon_{\mathcal{A}}$ with $\beta = k_BT$. Nonetheless, we do not calculate the supercurrent by this method and only focus our discussions on the analyses of the Andreev bound states. To simplify the bound state expression Eq. (12), we first set $\Delta_l = \Delta_r = \Delta$ and $h_r = h_l = 0$ and consequently find

$$\varepsilon_{\mathcal{A}} = \Delta\cos\varphi/2. \tag{13}$$

This relation shows that the bound state at $\varphi = 0$ moves to the edge of superconducting gap at $\varepsilon_{\mathcal{A}} = \Delta$ and to zero energy when $\varphi = \pi$ in line with previous works on the conventional Josephson short junctions [55–58]. These results are consistent with our numerical calculations discussed in Fig. 4(a). We now set h_l,$h_r \neq 0$ and find the following relation for the Andreev bound states:

$$\varepsilon_{\mathcal{A}} = \frac{\mathcal{H}_+(1-\cos\varphi) \pm \sin\varphi\sqrt{2\Delta^2(1-\cos\varphi)-\mathcal{H}_-^2}}{2(1-\cos\varphi)}. \tag{14}$$

We see that the general aspects of the latter expression are in full agreement with the numerical results presented in Figs. 4(b) and 4(c). If we set $\varphi = \pi$, the bound state occurs at $\varepsilon_{\mathcal{A}} = (h_l + h_r)/2$. It is evident that if the magnetization directions in the left and right segments are oppose, $h_l = -h_r$, the bound state takes place at $\varepsilon = 0$ which is consistent with the DOS results presented in Fig. 4(c). The difference between the TI junction and a conventional one is the presence of strong spin-orbit coupling (or equivalently the spin-momentum locking), and therefore, the directional dependence discussed above is a direct consequence of the spin-momentum locking phenomenon. It is worth noting that not only can the DOS in an intrinsic spin-orbit coupled magnetic superconducting hybrid be magnetization direction dependent, but also the charge and spin supercurrents are found to be sensitive to the direction of magnetization [19–22,74]. The DOS at maximum superconducting phase difference $\varphi = \pi$ in a diffusive Josephson junction peaks at zero energy due to the appearance of superconducting triplet correlations both in magnetic inhomogeneous [75] and spin-orbit coupled systems [74].

The spontaneous supercurrent explored here can be experimentally measurable through multiterminal devices [76]. Two transverse electrodes should be attached to the lateral edges of the two-dimensional topological insulator weak-link at $x = 0$ and $y = \pm W/2$ where W is the junction width and we assumed $W \to \infty$ in our calculations (see Fig. 1). The transverse spontaneous current parallel to the junction interface discussed above injects charge current into the lateral leads and can induce a voltage drop between the lateral leads that is detectable in experiment [76]. By applying a voltage difference between these lateral electrodes, the DOS and thus the subgap bound states can be revealed in an I-V measurement. When these signatures are detected in an experiment, a rotatable in-plane external magnetic field can confirm our findings. Our predictions are valid regardless of the density/strength of nonmagnetic impurity and scattering resources present at the surface channels. Also, to rotate the magnetization in the setup proposed, an in-plane external magnetic field suffices. Therefore, the impurity and Meissner obstacles pointed out in the introduction to experimentally observe the spontaneous currents at the surfaces of chiral superconductors are not relevant in the Josephson weak-link considered in this paper.

III. CONCLUSIONS

In conclusion, utilizing a recently generalized quasiclassical approach to superconducting magnetized surface states of a three-dimensional topological insulator (TI) [26], we study supercurrent flows at the magnetic interface of a TI. We consider a Josephson weak-link with two uniformly in-plane magnetized segments, $\boldsymbol{h}_l$ and $\boldsymbol{h}_r$, where the magnetizations have nonzero components perpendicular to the interface. Our results reveal that a spontaneous supercurrent flows parallel to the interface at the junction location provided that $|\boldsymbol{h}_l| \neq |\boldsymbol{h}_r|$ and reaches its maximum when the phase difference φ between the left and right segments is close to π. We also study the Andreev bound states in such a weak-link through the density of states both numerically and analytically. We Riccati-parametrize the Green's function involved in our calculations and derive analytical expressions to the Andreev subgap states. We discuss the influences of the magnetization directions in the left and right sides of the Josephson weak-link on the Andreev bound states.

ACKNOWLEDGMENTS

M.A. is thankful to I. V. Bobkova and A. M. Bobkov for useful discussions. M.A. is supported by Iran's National Elites Foundation (INEF).

[1] M. Z. Hasan and C. L. Kane, Colloquium: Topological insulators, Rev. Mod. Phys. **82**, 3045 (2010).

[2] X.-L. Qi and S.-C. Zhang, Topological insulators and superconductors, Rev. Mod. Phys. **83**, 1057 (2011).

[3] G. E. Volovik, *The Universe in a Helium Droplet* (Oxford University Press, Oxford, 2003).

[4] J. R. Williams, A. J. Bestwick, P. Gallagher, S. S. Hong, Y. Cui, A. S. Bleich, J. G. Analytis, I. R. Fisher, and D.

Goldhaber-Gordon, Unconventional Josephson Effect in Hybrid Superconductor–Topological Insulator Devices, Phys. Rev. Lett. **109**, 056803 (2012).

[5] M. Veldhorst, M. Snelder, M. Hoek, T. Gang, V. K. Guduru, X. L. Wang, U. Zeitler, W. G. van der Wiel, A. A. Golubov, H. Hilgenkamp, and A. Brinkman, Josephson supercurrent through a topological insulator surface state, Nat. Mater. **11**, 417 (2012).

[6] L. Galletti, S. Charpentier, M. Iavarone, P. Lucignano, D. Massarotti, R. Arpaia, Y. Suzuki, K. Kadowaki, T. Bauch, A. Tagliacozzo, F. Tafuri, and F. Lombardi, Influence of topological edge states on the properties of $Al/Bi_2Se_3/Al$ hybrid Josephson devices, Phys. Rev. B **89**, 134512 (2014).

[7] K. C. Nowack, E. M. Spanton, M. Baenninger, M. Konig, J. R. Kirtley, B. Kalisky, C. Ames, P. Leubner, C. Brüne, H. Buhmann, L. W. Molenkamp, D. Goldhaber-Gordon, and K. A. Moler, Imaging currents in HgTe quantum wells in the quantum spin Hall regime, Nat. Mater. **12**, 787 (2013).

[8] E. M. Spanton, K. C. Nowack, L. Du, G. Sullivan, R.-R. Du, and K. A. Moler, Images of Edge Current in InAs/GaSb Quantum Wells, Phys. Rev. Lett. **113**, 026804 (2014).

[9] E. Y. Ma, M. R. Calvo, J. Wang, B. Lian, M. Mühlbauer, C. Brüne, Y.-T. Cui, K. Lai, W. Kundhikanjana, Y. Yang, M. Baenninger, M. Konig, C. Ames, H. Buhmann, P. Leubner, L. W. Molenkamp, S.-C. Zhang, D. Goldhaber-Gordon, M. A. Kelly, and Z.-X. Shen, Unexpected edge conduction in mercury telluride quantum wells under broken time-reversal symmetry, Nat. Commun. **6**, 7252 (2015).

[10] F. Pientka, A. Keselman, E. Berg, A. Yacoby, A. Stern, and B. I. Halperin, Topological Superconductivity in a Planar Josephson Junction, Phys. Rev. X **7**, 021032 (2017).

[11] A. S. Vasenko, A. A. Golubov, V. M. Silkin and E. V. Chulkov, Odd-frequency superconductivity induced in topological insulators with and without hexagonal warping, J. Phys.: Condens. Matter **29**, 295502 (2017).

[12] Q. Yu, Z. Tao, J. Song, Y. C. Tao, and J. Wang, Supercurrent switch in π topological junctions based upon a narrow quantum spin Hall insulator, Sci. Rep. **7**, 10723 (2017).

[13] A. S. Vasenko, A. A. Golubov, V. M. Silkin, and E. V. Chulkov, Unconventional pairing in three-dimensional topological insulators with warped surface state, JETP Lett. **105**, 497 (2017).

[14] F. S. Bergeret, A. F. Volkov, and K. B. Efetov, Odd triplet superconductivity and related phenomena in superconductor-ferromagnet structures, Rev. Mod. Phys. **77**, 1321 (2005).

[15] A. Buzdin, Proximity effects in superconductor-ferromagnet heterostructures, Rev. Mod. Phys. **77**, 935 (2005).

[16] A. Buzdin, Direct Coupling between Magnetism and Superconducting Current in the Josephson φ_0 Junction, Phys. Rev. Lett. **101**, 107005 (2008).

[17] S. Mironov and A. Buzdin, Spontaneous Currents in Superconducting Systems with Strong Spin-Orbit Coupling, Phys. Rev. Lett. **118**, 077001 (2017).

[18] I. V. Bobkova and Yu. S. Barash, Effects of spin-orbit interaction on superconductor-ferromagnet heterostructures: Spontaneous electric and spin surface currents, JETP Lett. **80**, 494 (2004).

[19] F. Konschelle, I. V. Tokatly, and F. S. Bergeret, Ballistic Josephson junctions in the presence of generic spin dependent fields, Phys. Rev. B **94**, 014515 (2016).

[20] F. Konschelle, Transport equations for superconductors in the presence of spin interaction, Eur. Phys. J. B **87**, 119 (2014).

[21] M. Alidoust and K. Halterman, Spontaneous edge accumulation of spin currents in finite-size two-dimensional diffusive spin-orbit coupled SFS heterostructures, New J. Phys. **17**, 033001 (2015).

[22] M. Alidoust and K. Halterman, Long-range spin-triplet correlations and edge spin currents in diffusive spin-orbit coupled SNS hybrids with a single spin-active interface, J. Phys: Condens. Matter **27**, 235301 (2015).

[23] R. Beiranvand, H. Hamzehpour, and M. Alidoust, Nonlocal Andreev entanglements and triplet correlations in graphene with spin-orbit coupling, Phys. Rev. B **96**, 161403(R) (2017).

[24] A. A. Burkov and D. G. Hawthorn, Spin and Charge Transport on the Surface of a Topological Insulator, Phys. Rev. Lett. **105**, 066802 (2010).

[25] C. Kurter, A. D. K. Finck, Y. S. Hor, and D. J. Van Harlingen, Evidence for an anomalous current-phase relation in topological insulator Josephson junctions, Nat. Commun. **6**, 7130 (2015).

[26] A. Zyuzin, M. Alidoust, and D. Loss, Josephson junction through a disordered topological insulator with helical magnetization, Phys. Rev. B **93**, 214502 (2016).

[27] I. V. Bobkova, A. M. Bobkov, A. A. Zyuzin, and M. Alidoust, Magnetoelectrics in disordered topological insulator Josephson junctions, Phys. Rev. B **94**, 134506 (2016).

[28] M. Alidoust and K. Halterman, Proximity induced vortices and long-range triplet supercurrents in ferromagnetic Josephson junctions and spin valves, J. Appl. Phys. **117**, 123906 (2015).

[29] I. Sochnikov, L. Maier, C. A. Watson, J. R. Kirtley, C. Gould, G. Tkachov, E. M. Hankiewicz, C. Brüne, H. Buhmann, L. W. Molenkamp, and K. A. Moler, Nonsinusoidal Current Phase Relationship in Josephson Junctions from the 3D Topological Insulator HgTe, Phys. Rev. Lett. **114**, 066801 (2015).

[30] J. B. Oostinga, L. Maier, P. Schuffelgen, D. Knott, C. Ames, C. Brüne, G. Tkachov, H. Buhmann, and L. W. Molenkamp, Josephson Supercurrent through the Topological Surface States of Strained Bulk HgTe, Phys. Rev. X **3**, 021007 (2013).

[31] F. Dolcini, M. Houzet, and J. S. Meyer, Topological Josephson φ_0 junctions, Phys. Rev. B **92**, 035428 (2015).

[32] M. Shiranzaei, F. Parhizgar, J. Fransson, H. Cheraghchi, Impurity scattering on the surface of topological insulator thin films, Phys. Rev. B **95**, 235429 (2017).

[33] A. G. Mal'shukov, Long-range effect of a Zeeman field on the electric current through the helical metal-superconductor interface in Andreev interferometer, arXiv:1707.08335.

[34] E. G. Volovik, Quantum Hall state and chiral edge state in thin 3He-A film, JETP Lett. **55**, 368 (1992).

[35] V. P. Mineev and K. V. Samokhin, *Introduction to Unconventional Superconductivity* (Gordon and Breach, Amsterdam, 1999).

[36] A. Frusaki, M. Matsumoto, and M. Sigrist, Spontaneous Hall effect in a chiral p-wave superconductor, Phys. Rev. B **64**, 054514 (2001).

[37] Yu. S. Barash, A. M. Bobkov, and M. Fogelström, Josephson current between chiral superconductors, Phys. Rev. B **64**, 214503 (2001).

[38] P. E. C. Ashby and C. Kallin, Suppression of spontaneous supercurrents in a chiral p-wave superconductor, Phys. Rev. B **79**, 224509 (2009).

[39] M. Sigrist and K. Ueda, Phenomenological theory of unconventional superconductivity, Rev. Mod. Phys. **63**, 239 (1991).

[40] A. P. Mackenzie and Y. Maeno, The superconductivity of Sr_2RuO_4 and the physics of spin-triplet pairing, Rev. Mod. Phys. **75**, 657 (2003).

[41] M. Smidman, M. B. Salamon, H. Q. Yuan, and D. F. Agterberg, Superconductivity and spin-orbit coupling in non-centrosymmetric materials, Rep. Prog. Phys. **80**, 036501 (2017).

[42] R. Nandkishore, L. S. Levitov, and A. V. Chubukov, Chiral superconductivity from repulsive interactions in doped graphene, Nat. Phys. **8**, 158 (2012).

[43] M. L. Kiesel, C. Platt, W. Hanke, and R. Thomale, Model Evidence of an Anisotropic Chiral $d + id$-Wave Pairing State for the Water-Intercalated $Na_xCoO_2 \cdot yH_2O$ Superconductor, Phys. Rev. Lett. **111**, 097001 (2013).

[44] P. G. Bjornsson, Y. Maeno, M. E. Huber, and K. A. Moler, Scanning magnetic imaging of Sr_2RuO_4, Phys. Rev. B **72**, 012504 (2005).

[45] J. R. Kirtley, C. Kallin, C. W. Hicks, E.-A. Kim, Y. Liu, K. A. Moler, Y. Maeno, and K. D. Nelson, Upper limit on spontaneous supercurrents in Sr_2RuO_4, Phys. Rev. B **76**, 014526 (2007).

[46] Y. Tada, W. Nie, and M. Oshikawa, Orbital Angular Momentum and Spectral Flow in Two-Dimensional Chiral Superfluids, Phys. Rev. Lett. **114**, 195301 (2015).

[47] M. H. S. Amin, A. N. Omelyanchouk, and A. M. Zagoskin, Mechanisms of spontaneous current generation in an inhomogeneous d-wave superconductor, Phys. Rev. B **63**, 212502 (2001).

[48] K. Kuboki and H. Takahashi, Spontaneous spin current near the interface between unconventional superconductors and ferromagnets, Phys. Rev. B **70**, 214524 (2004).

[49] S. V. Bakurskiy, N. V. Klenov, I. I. Soloviev, M. Yu. Kupriyanov, and A. A. Golubov, Observability of surface currents in p-wave superconductors, Supercond. Sci. Technol. **30**, 044005 (2017).

[50] S.-I. Suzuki and Y. Asano, Spontaneous edge current in a small chiral superconductor with a rough surface, Phys. Rev. B **94**, 155302 (2016).

[51] P. M. R. Brydon, C. Iniotakis, and D. Manske, The chiral superconductor-ferromagnet-chiral superconductor Josephson junction, New J. Phys. **11**, 055055 (2009).

[52] A. Srivastava *et al.*, Magnetization-control and transfer of spin-polarized Cooper pairs into a half-metal manganite, arXiv:1706.00332.

[53] K. D. Usadel, Generalized Diffusion Equation for Superconducting Alloys, Phys. Rev. Lett. **25**, 507 (1970).

[54] G. Eilenberger, Transformation of Gorkov's equation for type II superconductors into transport-like equations, Z. Phys. **214**, 195 (1968).

[55] I. O. Kulik, Magnitude of the critical Josephson tunnel current, JETP **22**, 841 (1966).

[56] L. N. Bulaevskii, V. V. Kuzii, and A. A. Sobyanin, Superconducting system with weak coupling to the current in the ground state, JETP Lett. **25**, 290 (1977).

[57] I. O. Kulik and A. N. Omel'yanchuk, Josephson effect in superconductive bridges: Microscopic theory, Fiz. Nizk. Temp. **4**, 296 (1978) [Sov. J. Low Temp. Phys. **4**, 142 (1978)].

[58] A. A. Golubov, M. Yu. Kupriyanov, and E. Il'ichev, The current-phase relation in Josephson junctions, Rev. Mod. Phys. **76**, 411 (2004).

[59] M. Alidoust, A. Zyuzin, and K. Halterman, Pure odd frequency superconductivity at the cores of proximity vortices, Phys. Rev. B **95**, 045115 (2017).

[60] I. V. Krive, A. M. Kadigrobov, R. I. Shekhter, and M. Jonson, Influence of the Rashba effect on the Josephson current through a superconductor/Luttinger liquid/superconductor tunnel junction, Phys. Rev. B **71**, 214516 (2005).

[61] A. Brunetti, A. Zazunov, A. Kundu, and R. Egger, Anomalous Josephson current, incipient time-reversal symmetry breaking, and Majorana bound states in interacting multilevel dots, Phys. Rev. B **88**, 144515 (2013).

[62] M. Alidoust and J. Linder, φ_0-state and inverted Fraunhofer pattern in nonaligned Josephson junctions, Phys. Rev. B **87**, 060503(R) (2013).

[63] D. M. Heim, N. G. Pugach, M. Yu. Kupriyanov, E. Goldobin, D. Koelle and R. Kleiner, Ferromagnetic planar Josephson junction with transparent interfaces: A φ junction proposal, J. Phys.: Condens. Matter **25**, 239601 (2013).

[64] D. Feinberg and C. A. Balseiro, Spontaneous vortex state and ϕ-junction in a superconducting bijunction with a localized spin, Phys. Rev. B **90**, 075432 (2014).

[65] E. Goldobin, D. Koelle, and R. Kleiner, Tunable $\pm\varphi$, φ_0, and $\varphi_0 \pm \varphi$ Josephson junction, Phys. Rev. B **91**, 214511 (2015).

[66] M. A. Silaev, θ_0 thermal Josephson junction, Phys. Rev. B **96**, 064519 (2017).

[67] I. V. Bobkova, A. M. Bobkov, and M. A. Silaev, Gauge theory of the long-range proximity effect and spontaneous currents in superconducting heterostructures with strong ferromagnets, Phys. Rev. B **96**, 094506 (2017).

[68] M. A. Silaev, I. V. Tokatly, and F. S. Bergeret, Anomalous current in diffusive ferromagnetic Josephson junctions, Phys. Rev. B **95**, 184508 (2017).

[69] C. Schrade, S. Hoffman, and D. Loss, Detecting topological superconductivity with φ_0-Josephson junctions, Phys. Rev. B **95**, 195421 (2017).

[70] D. S. Shapiro, D. E. Feldman, A. D. Mirlin, and A. Shnirman, Thermoelectric transport in junctions of Majorana and Dirac channels, Phys. Rev. B **95**, 195425 (2017).

[71] A. A. Reynoso, G. Usaj, C. A. Balseiro, D. Feinberg, and M. Avignon, Anomalous Josephson Current in Junctions with Spin Polarizing Quantum Point Contacts, Phys. Rev. Lett. **101**, 107001 (2008).

[72] D. B. Szombati, S. Nadj-Perge, D. Car, S. R. Plissard, E. P. A. M. Bakkers, and L. P. Kouwenhoven, Josephson φ_0-junction in nanowire quantum dots, Nat. Phys. **12**, 568 (2016).

[73] N. Schopol, Transformation of the Eilenberger equations of superconductivity to a scalar Riccati equation, arXiv:cond-mat/9804064.

[74] S. H. Jacobsen, J. A. Ouassou, and J. Linder, Critical temperature and tunneling spectroscopy of superconductor-ferromagnet hybrids with intrinsic Rashba-Dresselhaus spin-orbit coupling, Phys. Rev. B **92**, 024510 (2015).

[75] M. Alidoust, G. Rashedi, J. Linder, and A. Sudbø, Phase-controlled proximity effect in ferromagnetic Josephson junctions: Calculation of the density of states and the electronic specific heat, Phys. Rev. B **82**, 014532 (2010).

[76] J. Wunderlich, B. G. Park, A. C. Irvine, L. P. Zarbo, E. Rozkotova, P. Nemec, V. Novak, J. Sinova, and T. Jungwirth, Spin Hall effect transistor, Science **330**, 1801 (2010).